Research Square

Preprints are preliminary reports that have not undergone peer review.
They should not be considered conclusive, used to inform clinical practice,
or referenced by the media as validated information.

Molecular Dynamics and Energetic Performance of PBX Explosives Containing Al-Li Alloys via Binder and Content Regulation

Yi Zhang
Academy of Military Medical Sciences
Zhihong Yu
Academy of Military Medical Sciences
Hanqing Xu
Academy of Military Medical Sciences
Liang Zhou
Academy of Military Medical Sciences
Hao Chen
Academy of Military Medical Sciences
Xinggao Zhang
Academy of Military Medical Sciences
Zhihua Zhuang
zhihua0802@163.com

Academy of Military Medical Sciences

Research Article

Keywords: PBX explosive, Molecular dynamics, binder, Aluminium-lithium alloy

Posted Date: November 10th, 2026

DOI: https://doi.org/10.21203/rs.3.rs-11342663/v1

License: This work is licensed under a Creative Commons Attribution 4.0 International License.
Read Full License

Additional Declarations: No competing interests reported.

Molecular Dynamics and Energetic Performance of PBX Explosives Containing Al-Li Alloys via Binder and Content Regulation

Yi Zhang[#], Zhihong Yu[#], Hanqing Xu, Liang Zhou, Hao Chen*, Xinggao Zhang, and Zhihua Zhuang*

Chemical Defense Institute, Academy of Military Sciences, Beijing 102205, China.

#These authors are co-first authors of the article.

*Corresponding author: chen1274061939@163.com (Hao Chen)

*Corresponding author: zhihua0802@163.com (Zhihua Zhuang)

Molecular Dynamics and Energetic Performance of PBX Explosives Containing Al-Li Alloys via Binder and Content Regulation

Abstract

To clarify the molecular-scale synergistic mechanism of the dual-layer wax-binder coating interface governing the safety and energy characteristics of Al-Li alloy modified HMX-based composite explosives, systematic molecular dynamics (MD) simulations are performed within MATERIALS STUDIO 2023. Three series of sandwich-structured models, including HMX/Wax/Binder, AP/Wax/Binder, and Al-Li alloy/Wax/binder systems with gradient lithium concentrations, are constructed sequentially. Miscibility between microcrystalline wax and four typical energetic binders, binding energy (E_{bind}), and cohesive energy density (CED) are quantitatively evaluated. EXPLO-5 software is adopted to compute the theoretical detonation performance metrics of corresponding explosive formulations at varying lithium doping ratios. The results demonstrate that F_{2604} emerges as the optimal binder as the optimal adhesive, exhibits good compatibility with wax. It possesses both a high interfacial E_{bind} of 13261 kJ·mol^{-1}, a CED of 6.03×10^{8} kJ·cm^{-3} and shortening HMX average N-NO_2 trigger bond length by 4.23%, while the system with 3% lithium doping exhibits the highest molecular packing density and balanced comprehensive performance. Following formulation optimisation, HMX/AP/Al-3Li composite explosive, as Al-to-oxygen ratio ($R_{Al/O}$) rises, more AP-supplied reactive oxygen improves metal fuel reaction efficiency, forming a trend of decreasing heat of detonation, increasing detonation velocity, and both the explosion temperature and detonation pressure peak at $R_{Al/O}$ is 0.34 with the total generation of detonation gases at its minimum, which provides solid theoretical support for the molecular-level formulation design of high-energy low-sensitivity PBXs containing Al-Li alloys.

Keywords: PBX explosive; Molecular dynamics; binder; Aluminium-lithium alloy

1 Introduction

The energy performance, safety, and mechanical properties of polymer bonded explosives (PBXs) are governed not only by the energetic crystals themselves but also by the binders and functional additives coating the crystal surfaces [1]. Consequently, formulation design and interfacial structure regulation have long been research priorities. Octogen (HMX), a high-energy explosive widely used in propellants and military explosive formulations, is highly sensitive to mechanical stimuli such as impact and friction, readily forming hot spots that can lead to accidental initiation, which severely restricts its practical applications [1-2].

Surface coating modification of HMX crystals is an effective approach to reduce their sensitivity and enhance safety. By constructing a core-shell structure on the HMX surface, the coating layer can serve as an inert physical barrier that isolates external thermal and mechanical impacts and suppresses hot-spot formation, while the coating material itself also influences the overall mechanical properties. Currently, binders and microcrystalline wax are common and important materials for tailoring the interfacial properties of energetic components and building shell layers. Binders, such as fluoropolymers, convert impact energy into thermal energy through segmental motion of molecular chains and dissipate it, thereby improving thermal stability. For instance, Li et al. reported that coating HMX with F_{2602} increased its critical thermal explosion temperature from 271.79 °C to 283.25 °C [3]. Microcrystalline wax, on the other hand, reduces interparticle friction via a lubrication effect, allowing particles to slide rather than accumulate heat under mechanical stimuli, which is particularly effective in suppressing friction sensitivity, reducing the explosion probability by 40%. As matrix materials, binders provide mechanical support and buffering capacity, and their combination with paraffin-like substances further enhances the integrity and interfacial

lubricity of the coating layer [4-7]. A "sea urchin"-like structure constructed from graphite, BR, and microcrystalline wax coated on CL-20 was shown to reduce the explosion probabilities of friction and impact sensitivities to 36% and 38%, respectively, with an energy loss of no more than 3% [8]. When hexagonal boron nitride nanosheets (HBNNSs) were synergistically coated with ethylene-vinyl acetate copolymer (EVA) on HMX, they effectively impeded thermal shock and improved coating integrity, raising the H_{50} value to 65.3 cm [9].

In the optimization of explosive formulations, the incorporation of metal fuels is an effective strategy to enhance energy output. Particularly for aluminum-containing explosives, doping with highly reactive elements such as Li to form aluminum alloys has become an effective route to improve the reactivity of aluminum. Li can disrupt the alumina passivation film, lower the activation energy of oxidation reactions, and promote mass transfer and diffusion of liquid aluminum, ultimately resulting in faster and more concentrated high-temperature reaction rates [10-12]. Al-Li alloys theoretically possess higher combustion heat and reactivity than pure aluminum powder. Introducing Al-Li alloys into HMX-based PBX and constructing a dual-layer core-shell structure with microcrystalline wax and a binder is expected to improve the overall mechanical properties while enhancing the stability of the highly reactive Al-Li powder [13]. Li et al. achieved excellent encapsulation of paraffin wax (PW) via melt blending with low-density polyethylene (LDPE), which improved the system stability, and adding 15 wt% Al powder further increased the thermal conductivity of this encapsulated system by 67% [14]. Wang et al. performed fluorination modification on Al-5Li alloy powder via fluorosilane-epoxysilane coating followed by glycidyl azide polymer (GAP) grafting, which notably enhances the thermal stability, combustion performance and propellant compatibility of the Al-5Li powder [15]. However, the synergistic mechanism of this dual-layer interface at the molecular scale remains poorly understood, which limits the rational screening and optimization of coating formulations.

Molecular dynamics (MD) simulations offer a convenient means to investigate the optimization of shell materials and interfacial interactions [16-18]. Unlike previous simulations that focused solely on single-polymer coatings on energetic materials, this study performs MD simulations of interfacial interactions in HMX-based Al-Li alloy composite explosives with a dual-layer core-shell structure consisting of an inner microcrystalline wax (Hereinafter referred to as 'wax' in this study) layer and an outer polymer binder layer [19-23]. A core-double-shell PBX explosive microstructure is proposed and constructed, with three representative sandwich-structure simulation models established separately: HMX/Wax/Binder, AP/Wax/Binder, and Al-Li alloy/Wax/Binder. Four polymer binders commonly used in composite energetic materials, ethylene-vinyl acetate copolymer (EVA), fluororubber (F_{2604}), and cis-polybutadiene rubber (BR), Hydroxyl-terminated polybutadiene (HTPB) are selected as the outer shell materials, while wax serves as the inner shell. The compatibility of the wax-binder shell layer was systematically evaluated first, followed by a comprehensive investigation of the three sandwich systems covering cohesive energy density (CED), binding energy (E_{bind}), radial distribution function (RDF), trigger bond length, mechanical properties, and detonation performance. The goal is to unravel, at the molecular level, the regulatory mechanisms of the dual-layer interfacial structure on thermal stability, mechanical response, and energy release, thereby providing a theoretical basis for the design of novel high-energy, low-sensitivity PBX formulations.

2. Model construction

The crystal structure of HMX was retrieved from the Cambridge Crystallographic Data Centre (CCDC 792934). The BFDH morphological prediction method was then applied to identify the most thermodynamically favorable growth face, which was determined to be the (0 1 1) crystal plane. To achieve a more accurate representation of interfacial interactions in subsequent simulations, the identified dominant crystal face of the HMX unit cell was cleaved and extended to form an 8 × 8 × 8 supercell.

In the preparation of PBX composite explosives, researchers typically subject the highly sensitive components to

a passivation process, namely by coating HMX and AP with wax. Subsequently, HMX, AP and metal powder are kneaded together using a binder, thereby forming a binder-encapsulated composite microstructure. Based on the actual composite structure of PBX composite explosives, as shown in Figure 1, three sandwich-structure models were identified for specific modelling and computational analysis: HMX/Wax/Binder; AP/Wax/Binder; and Al–Li alloy/Wax/Binder. A core-double-shell architecture was subsequently designed, in which the mass fraction of wax relative to energetic molecules (HMX or AP) matrix was 1%, whilst the mass fraction of each of the four binders was 3% of the total mass. The Build polymer module was used to polymerise the monomers of each binder into continuous bonding chains [24-25]. The Build layer module was then used to combine the HMX (or AP) supercell with the wax and adhesive models to form a sandwich-structure model in which the wax is directly attached to the outer surface of the HMX, whilst the polymer adhesive envelops the wax layer. Given that, during the manufacture of the PBX, the binder directly coats the Al-Li alloy, with the wax forming the outermost layer, a model of the Al - Li alloy/binder/Wax structure was established based on the actual circumstances.

The above model, with all calculations carried out under the COMPASS III [26] force field. Geometry optimization was performed with a 50,000-iteration maximum, where the system was constrained at 10^{-4} GPa external pressure. The optimized systems underwent 500 ps low-temperature NVT relaxation at 100 K using the Berendsen thermostat with a 0.1 fs time step, with Gaussian-distributed random initial velocities to eliminate high-energy disturbances to the energetic crystal framework. The relaxed models were subsequently transferred to 298 K, 10^{-4} GPa NPT ensemble for 1 ns equilibrium production with Berendsen thermostat-barostat dual control, which preserves skeleton and interface integrity and ensures rapid convergence to experiment-consistent equilibrated configurations. Electrostatic interactions were computed via Ewald summation, while van der Waals interactions adopted the Atom-based scheme with a unified 12.5 Å cutoff radius.

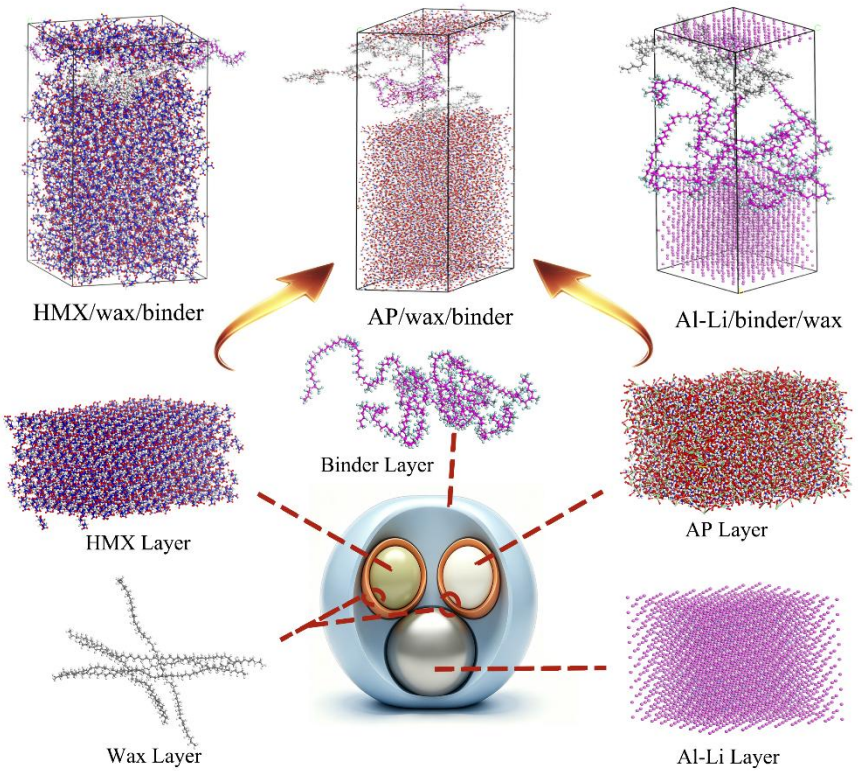


Fig. 1 Schematic diagram of HMX-based polymer bonded explosive layered model construction.

3 Results and discussion

3.1 Compatibility analysis

3.1.1 Blends module compatibility predictions of Wax/Binder shell

For double-layer core-shell energetic microspheres, the wax-binder composite shell forms a continuous molecular-scale interface wrapping the inner energetic components. Favorable miscibility, intrinsically governed by the components' intermolecular interaction strength and uniformity, eliminates molecular phase demixing thermodynamic driving force, locking the shell in a homogeneous, defect-free microstructure. This uniform intermolecular landscape evenly distributes non-covalent interaction sites across the shell volume, building a continuous constraint field that suppresses adjacent core energetic species' molecular mobility, reducing the likelihood of hotspots forming. This work employs the Blends molecular dynamics module to predict wax-binder miscibility, establishing a computational framework for molecular-scale optimal shell preliminary component screening.

All intermolecular interaction strength calculations for the wax-binder pair were completed via the Blends module, whose underlying framework is fully built on Flory-Huggins thermodynamic theory [27]. This module quantifies miscibility and phase behavior of binary polymer blends by deriving interaction parameters and volume fractions of the two components. In the Flory-Huggins framework, the core interaction parameter χ is intrinsically temperature-dependent, correlated to mixing energy, Boltzmann constant and absolute temperature. Its thermodynamic definition is as follows:

$$\chi = \frac{E_{\mathrm{mix}}}{K_{\mathrm{b}} T} \tag{1}$$

Where E_{mix} denotes the mixing energy, the net free energy difference between the intermolecular interaction-dominated blended state and the sum of free energies of the two individual pure components, k_b is the Boltzmann constant, and T represents the absolute thermodynamic temperature of the system. A low or negative χ at target operating temperatures confirms favorable mutual molecular affinity, while a large positive χ indicates a thermodynamic tendency for homo-molecular aggregation. When χ exceeds the critical threshold, unfavorable mixing enthalpy will overcome the combinatorial entropy effect, triggering irreversible macroscopic phase separation inside the shell.

The binding energy distribution profile is applied as an auxiliary verification metric to calibrate the χ-derived miscibility conclusion. Highly overlapping distribution curves at the molecular level confirm uniform mixing of the two components, while distinct mismatched peaks directly signal poor miscibility and hidden phase separation risks. Here, wax was defined as the base matrix and the binder as the test component, with the resulting binding energy distribution curve and χ-temperature evolution curve presented in Fig. 2 and Fig. 3 respectively.

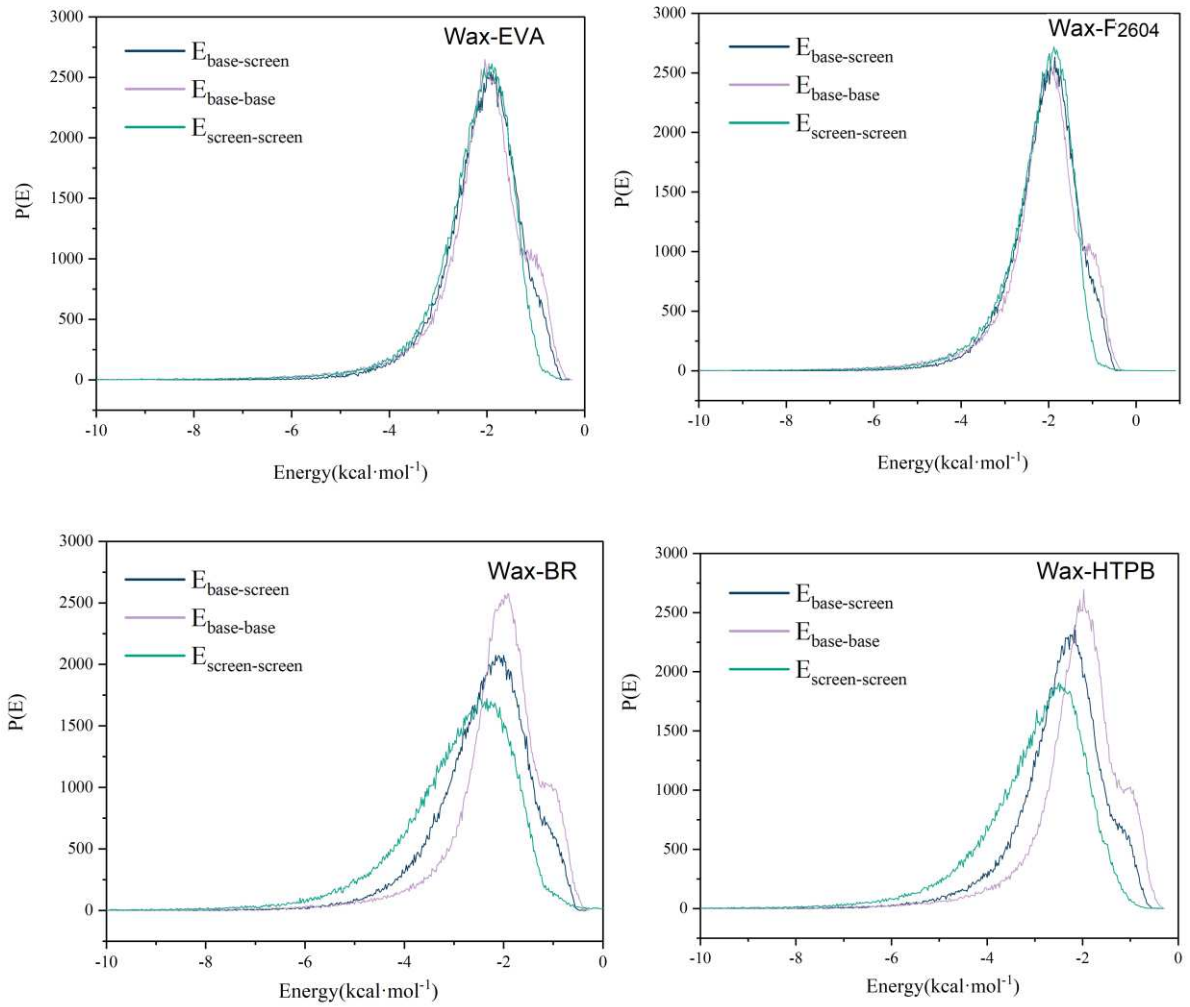


Fig. 2 Binding Energy Distribution Curve of the Wax-Binder

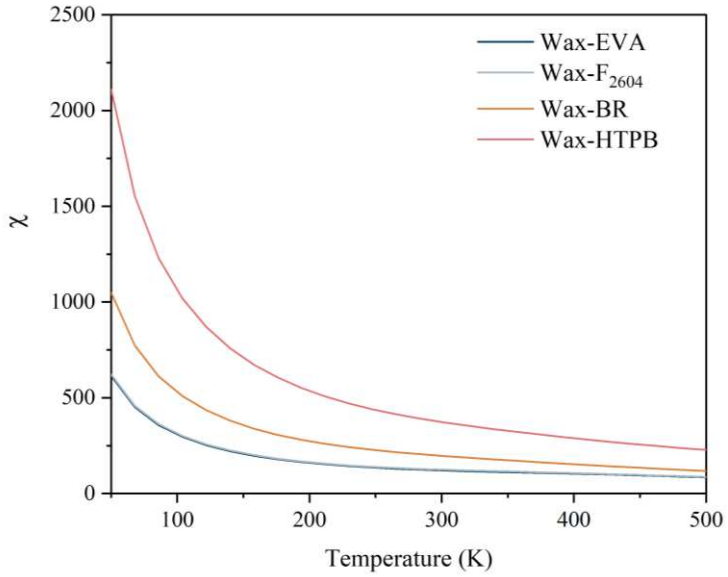


Fig. 3 χ-Temperature Curve of Wax-Binder System

From the Wax-Binder binding energy distribution curve, it can be preliminarily analyzed that the distribution curves of EVA, F_{2604} and wax components are relatively similar, and it is predicted that they are more likely to mix

and contact with the wax layer, while the component curves of BR, HTPB and wax show a relatively large gap, which means a poorer mixing compatibility. From the Wax-Binder interaction parameter χ-temperature curve, it can be more clearly concluded that as the temperature increases, the χ value between the two components tends to 0, indicating that under the action of temperature rise, the interaction between the two components will be enhanced, mixing and compatibility will be easier, and the χ value is smaller at room temperature (298 K), this result is the confirmation of the above preliminary analysis, and further proves that at this temperature, there is a good interaction between the two molecules, the mixing compatibility is better, and it is more conducive to the formation of a stable shell structure.

3.1.2 Binding energy (E_{bind}) and cohesive energy density (CED)

Binding energy (E_{bind}) quantitatively characterizes the strength of intermolecular interactions and serves as a core driving parameter for molecular assembly behavior. It is defined as the negative value of the system's interaction energy. In this work, the total number of molecules in all models was kept nearly identical to avoid additional normalization processing. A higher binding energy value indicates stronger interactions between components, better stability of the energetic system, and correspondingly higher potential to form a stable eutectic structure [28-29]. The calculation formula of binding energy in this study is as follows:

$$E_{\text{bind}} = -E_{\text{interaction}} = -\left(E_{\text{total}} - E_{\text{Wax}} - E_{\text{Binder}}\right) \tag{2}$$

The interfacial interaction strength between binder-Wax coating and energetic crystals is a core microscopic parameter that determines the interfacial adhesion stability, mechanical homogeneity, and long-term storage safety of composite energetic systems. Cohesive energy density (CED) is a core index characterizing thermodynamic stability, defined as the energy per unit volume required to vaporize 1 mole of condensed material into gaseous molecules [30-31]. This parameter quantifies the energy barrier needed to overcome intermolecular forces, a higher value means more energy is absorbed during vaporization, which creates a stronger hindrance to the thermal decomposition and detonation process of the material. In molecular dynamics simulations, the cohesive energy density can be directly calculated as the sum of van der Waals force and electrostatic force components, and the corresponding calculation formula is:

$$CED = E_{\text{ELE}} + E_{\text{VDW}} \tag{3}$$

Combined analysis of E_{bind} and CED can fully characterize both the total intermolecular driving force and per-volume interfacial adhesion strength of composite energetic systems, effectively eliminating performance misjudgment caused by single-indicator evaluation. This joint method is adopted to screen the optimal binder component suitable for the Al-Li alloy-energetic particle composite system, based on molecular dynamics simulation results of 8 ternary HMX-based and AP-based sandwich models listed in Table 1.

As shown in Fig. 4a, all four HMX-based systems present a narrow total CED range of 5.72×10^8-6.03×10^8 kJ·cm^{-3}, with van der Waals CED fluctuation below 1.4%, indicating nearly identical non-polar intermolecular contact density across four HMX/Wax/Bind interfaces. The slight CED discrepancy is entirely determined by the electrostatic contribution: the HMX/Wax/F_{2604} system reaches the maximum CED of 6.03×10^8 kJ·cm^{-3} and the E_{bind} also shows the same trend, reaching a maximum of 13260.77 kJ·mol^{-1}, originated from the directional dipole-dipole interaction between fluorine polar groups on F_{2604} chains and weak-polar end sites of wax molecular chains.

For AP-based systems in Fig. 4b, all models follow the interaction nature of ionic crystal interfaces, where electrostatic CED contributes over 97% to the total value. Their overall CED ranges from 9.05×10^9 to 1.14×10^{10} kJ·cm^{-3}, 15-19 times that of HMX-based systems. This order-of-magnitude superiority comes from the strong directional electrostatic adsorption between exposed polar ammonium/perchlorate sites on AP surface and polar

groups of wax and binder molecules. The AP/Wax/F_{2604} system achieves the maximum total CED of 1.14×10^{10} kJ·cm^{-3} along with the top van der Waals CED of 3.35×10^{8} kJ·cm^{-3} in this series. It is the only sample that synchronously maximizes both electrostatic and van der Waals interactions, avoiding the unbalanced performance defect in other AP-based systems. This system also obtains the maximum binding energy of 2671.82 kJ·mol^{-1}, 42.7% higher than the lowest HTPB system, which further quantitatively confirms its optimal interfacial bonding strength.

Consistent results from both HMX and AP systems confirm that F_{2604} is the only binder with simultaneously high E_{bind} and maximum per-volume CED, eliminating the flaw of pseudo-high total energy but insufficient interfacial strength, and meets the design requirement of synchronous high-adhesion coating for wax-coated HMX, AP and Al-Li particles. Lithium doping modification simulation in Fig. 4c further indicates that cohesion in 5 F_{2604}/Wax systems with different Li contents is completely dominated by van der Waals interaction, whose contribution exceeds 99.7%, while electrostatic component remains at a negligible 10^{5}-10^{6} kJ·cm^{-3} level. As Li content increases, E_{bind} and CED synchronously rise first and then decline, both reaching their peaks at the Al-3Li/F_{2604}/Wax sample (E_{bind} is 5250.61 kJ·mol^{-1}, CED is 5.68×10^{9} kJ·cm^{-3}). This synchronous variation excludes scale-related statistical error, proving that low-dose Li doping does not introduce extra strong electrostatic interactions, but adjusts F_{2604} chain conformation via weak Li-fluorine site interaction, reduces free volume pores during molecular stacking, and improves molecular packing density and effective van der Waals contact points per unit volume. Once Li content exceeds the critical threshold, non-specific aggregation of excess Li atoms forms dispersed local defects and damages the dense stacking structure, leading to simultaneous decrease of E_{bind} and CED. This quantitative result provides solid microscopic simulation support for determining the optimal Li doping ratio and balancing the interfacial performance and energy release characteristics of high-energy binder systems.

Table1. Binding Energy and CED for Three Energetic Composite Systems

Model	Average binding energy(kJ·mol^{-1})	Cohesive Energy Density(kJ·cm^{-3})	van der Waals Cohesive Energy Density(kJ·cm^{-3})	Electrostatic Cohesive Energy Density(kJ·cm^{-3})
HMX/Wax/EVA	5259.27	5.86×10^{8}	2.88×10^{8}	2.90×10^{8}
HMX/Wax/F_{2604}	13260.77	6.03×10^{8}	2.87×10^{8}	3.07×10^{8}
HMX/Wax/BR	4808.75	5.72×10^{8}	2.85×10^{8}	2.79×10^{8}
HMX/Wax/HTPB	3366.26	5.73×10^{8}	2.84×10^{8}	2.81×10^{8}
AP/Wax/EVA	1872.26	2.64×10^{8}	9.79×10^{9}	1.87×10^{3}
AP/Wax/F_{2604}	2671.82	3.35×10^{8}	1.17×10^{10}	2.67×10^{3}
AP/Wax/BR	2342.16	2.84×10^{8}	1.09×10^{10}	2.34×10^{3}
AP/Wax/HTPB	1866.63	2.44×10^{8}	9.29×10^{9}	1.87×10^{3}
Al-1Li/F_{2604}/Wax	4563.13	3.46×10^{9}	3.45×10^{9}	9.12×10^{5}
Al-2Li/F_{2604}/Wax	4993.08	5.52×10^{9}	5.49×10^{9}	2.19×10^{6}
Al-3Li/F_{2604}/Wax	5250.61	5.68×10^{9}	5.65×10^{9}	2.27×10^{6}
Al-4Li/F_{2604}/Wax	4849.60	4.68×10^{9}	4.65×10^{9}	2.30×10^{6}
Al-5Li/F_{2604}/Wax	4768.92	3.72×10^{9}	3.71×10^{9}	2.52×10^{6}

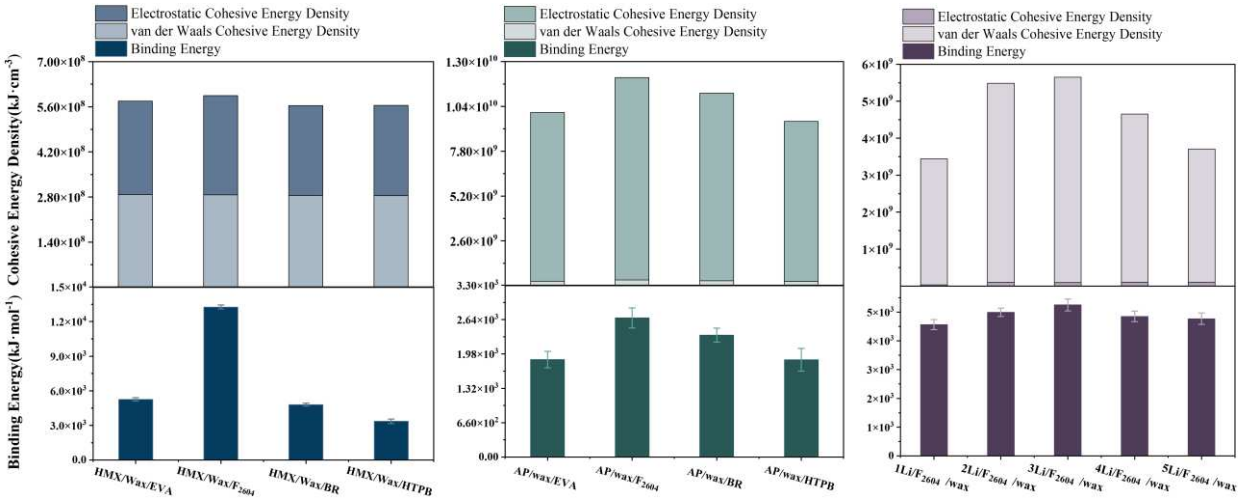


Fig. 4 Cohesive energy density (CED, Electrostatic and van der Waals contributions) and binding energy (E_{bind}) for three energetic composite systems. (a) HMX/Wax/Binder; (b) AP/Wax/Binder; (c) Al-Li alloy/Wax/Binder.

3.2 Radial distribution function

This study performs radial distribution function (RDF, *g(r)*) analysis on three types of interface models: HMX/Wax/Binder, AP/Wax/Binder, and Li-Al alloy/F_{2604}/Wax. The *g(r)* is defined as the normalized ratio of the local number density of hydrogen atoms in the spherical shell of radius r around the reference atom to the global average number density of hydrogen atoms in the entire system, which can directly characterize the spatial aggregation preference and interaction strength between characteristic atoms at the condensed-phase interface.

The nitro-oxygen atoms in HMX molecules, as well as the nitro-oxygen atoms and perchlorate oxygen atoms in AP molecules, are selected as strong-polarity hydrogen bond acceptors, while the corresponding hydrogen bond donor atoms refer to the hydrogen atoms in the wax phase and binder components. For the strong electronegative oxygen atoms in the EVA component and the strong electronegative fluorine atoms in the F_{2604} component, directional radial distribution functions with amino hydrogen in the energetic components as donors are additionally calculated. The classification of interaction force types adopts the general standards in this field: 1.5-2.2 Å corresponds to medium-strength hydrogen bonds, 2.2-3.2 Å corresponds to weak hydrogen bonds, and 3.2-5.0 Å corresponds to van der Waals interactions [32].

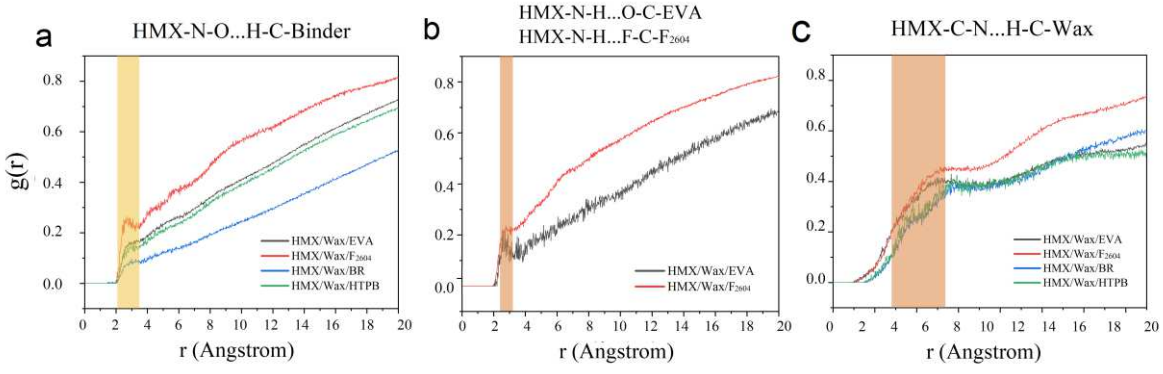


Fig.5 RDF of HMX-based sandwich models. (a) RDF of HMX-N-O…H-C-Binder. (b) RDF of HMX-N-H…O-C-EVA and HMX-N-H…F-C- F_{2604}. (c) RDF of HMX-C-N…H-C-Binder.

RDF for the HMX/Wax/Binder composite system are presented in Fig. 5. In Fig. 5a, the characteristic peaks of HMX nitro-oxygen and binder hydrogen are distributed in the range of 2.21-3.19 Å, which indicates that stable weak hydrogen bonds serve as the core interfacial binding force between HMX nitro-oxygen sites on this crystal plane and binder hydrogen atoms. Judging from the peak height, this effect is the most significant for F_{2604}. In Fig. 5b, the peak positions of HMX amino hydrogen and oxygen on the EVA carbon chain, as well as fluorine in F_{2604}, are concentrated in 2.39-3.29 Å, which still falls within the weak hydrogen bond region. In Fig. 5c, the characteristic peaks of nitrogen on the HMX ring and wax hydrogen are located in 3.77-4.83 Å, which belongs to the van der Waals interaction range. The abundant weakly polar sites ensure sufficient interfacial adhesion of the binder, and can also avoid local energy concentration caused by strong hydrogen bonds, thus reducing the potential risk of local hot spot sensitization at the contact interface. The peak heights follow the order of F_{2604}, EVA, HTPB, BR, indicating that binder components can regulate the interfacial binding strength between HMX and the wax phase through their own interfacial energy.

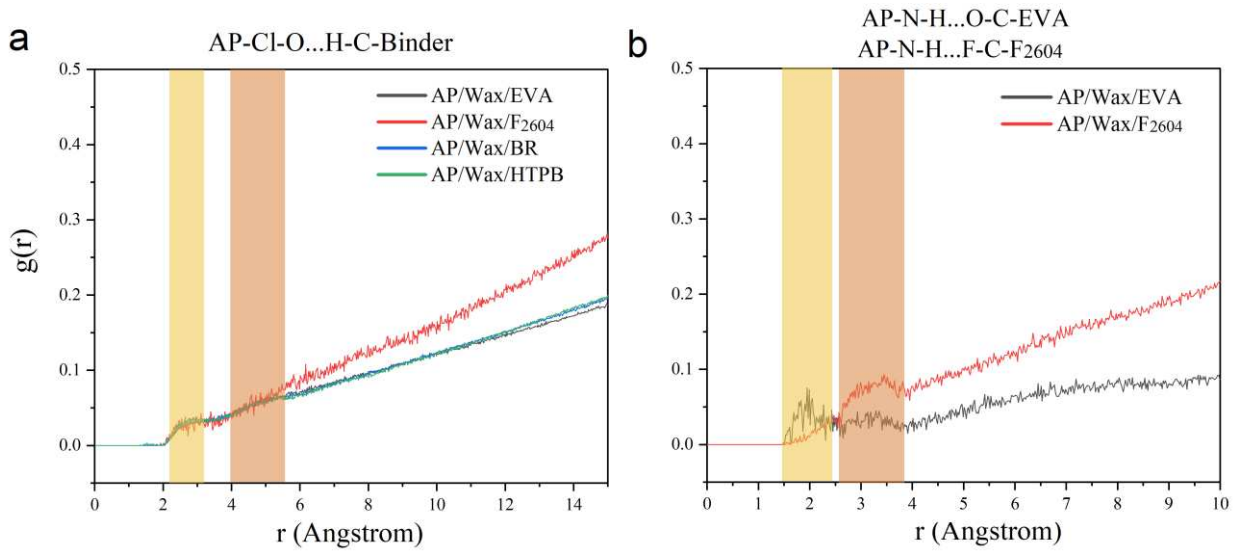


Fig.6 RDF of AP-based sandwich models. (a) RDF of AP Cl-O…H-C-Binder. (b) RDF of AP-N-H…O-C-EVA and AP-N-H…F-C-F_{2604}.

The RDF results for the AP/Wax/Binder system are shown in Fig. 6. In Fig. 6a, the interaction curves between AP perchlorate oxygen and the four binders present two distinct distribution intervals. The high-intensity peaks located at 2.09-3.03 Å fall within the weak hydrogen bond range, while the secondary peak at 4.01-5 Å corresponds to van der Waals interaction. This phenomenon indicates that the interfacial interaction strength between the polar

crystal plane of AP and the binder is higher than that of the aforementioned HMX system. The peak shape in this interval is noticeably broader, suggesting that the strong polarity of AP perchlorate may induce polarization of surrounding molecules on a larger spatial scale, making it easier to form an interfacial adsorption layer with a certain degree of long-range order.

For the EVA system, the two distinct peaks on its interaction curve, located at 1.65-2.19 Å and 3.21-3.77 Å, correspond to medium-strength hydrogen bonding and van der Waals interactions respectively. Oxygen-containing groups can form two-site cooperative adsorption with AP ammonium, reflecting the multi-dimensional interfacial binding feature. For the F_{2604} system, only one significant characteristic peak is observed, which is distributed in the 2.59-3.89 Å range and corresponds to the weak hydrogen bond region. This peak shape characteristic shows that the hydrogen bond acceptance capacity of F atoms interfacial interaction has a larger action radius and lower single-bond strength. This type of interaction mode is expected to endow the composite system with better impact resistance and buffering performance, reducing the possibility that a strong hydrogen bond network breaks instantaneously under overload conditions and further induces hot spot formation.

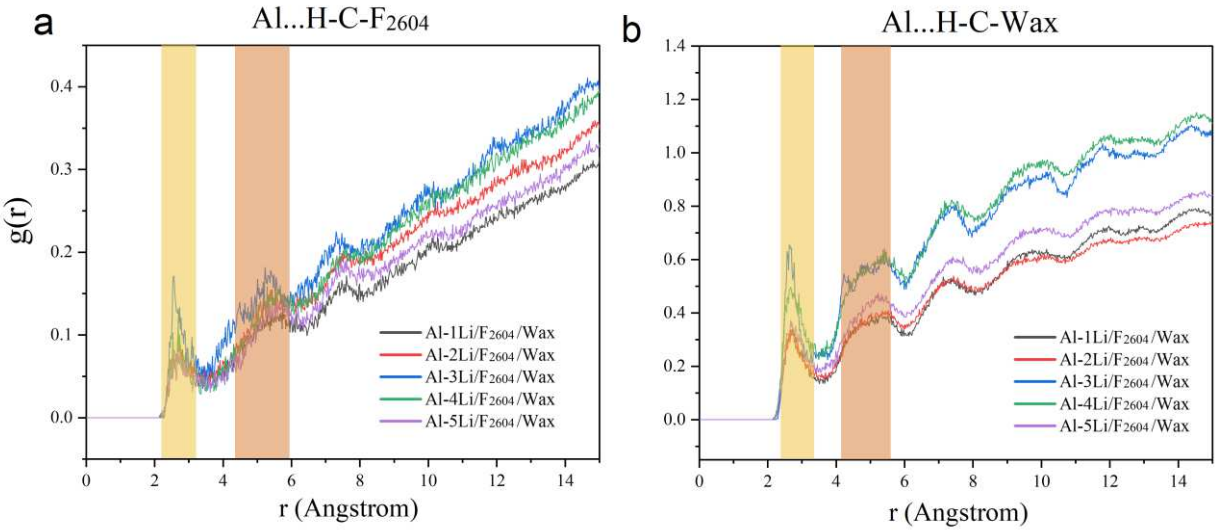


Fig.7 RDF of Al-Li alloys with different lithium contents. (a) RDF of Al…H-C- F_{2604}. (b) RDF of Al…H-C-Wax.

Based on the previously calculated results of binding energy and cohesive energy density, F_{2604} was identified as the binder with the best comprehensive interfacial performance. This component was further selected to carry out molecular dynamics simulations of interfacial interactions between Al-Li alloys with different lithium contents, and the corresponding radial distribution functions (RDF) were analyzed to evaluate the compatibility between aluminum-lithium alloys and energetic coating layers, show in the Fig.7. The results show that the characteristic peaks of Al atoms and hydrogen in F_{2604} molecules are distributed in the ranges of 2.21-2.77 Å and 4.39-5.9 Å

respectively, while the peak positions of Al atoms and hydrogen in Wax molecules fall in 2.35-3.25 Å and 4.01-5.13 Å. These ranges correspond to a synergistic interaction mechanism of weak hydrogen bonds and van der Waals forces. The intensities of all characteristic peaks corresponding to the Al-3Li sample are notably higher than those of the other four control systems (Al-1Li, Al-2Li, Al-4Li and Al-5Li). This indicates that there may exist an optimal threshold for lithium element doping: insufficient lithium content may not fully activate the surface aluminum sites, while excessive lithium content may induce phase transition of the surface oxide layer, which could reduce the interfacial adsorption activity instead. Providing direct microscopic support for the prediction of stability and energy output characteristics of Al-Li alloys containing composite explosives.

3.3 Trigger bond length

As the structural unit with the weakest chemical stability in energetic material molecules that undergoes homolytic cleavage preferentially under external energy input, the bond length evolution characteristic of the trigger bond serves as the core quantitative basis for revealing the sensitivity response law of desensitized composite systems from the molecular level. For typical nitramine high-energy explosives such as HMX, the N-NO_2 bond connecting the nitro group to the molecular skeleton is the widely recognized trigger bond responsible for decomposition and initiation. The bond length of this chemical bond directly reflects the interaction strength between the bonding atoms: a longer bond length means weaker mutual restraint between the N atom and the NO_2 group, lower bond dissociation activation energy, and higher tendency to dissociate under external stimuli such as mechanical force and shock, which will subsequently trigger the chained exothermic decomposition and correspond to higher mechanical sensitivity of the system [33].

Under the condition of a unified thermodynamic ensemble, equilibrium state calculations were carried out on the HMX unit cell of the most probable (0 1 1) crystal face and four groups of HMX/Wax/Binder systems composed of different binders. The Length distribution function in the Forcite Analysis module was used to statistically analyze all N-NO_2 trigger bonds of HMX molecules in each system, and the results are shown in Fig. 8.

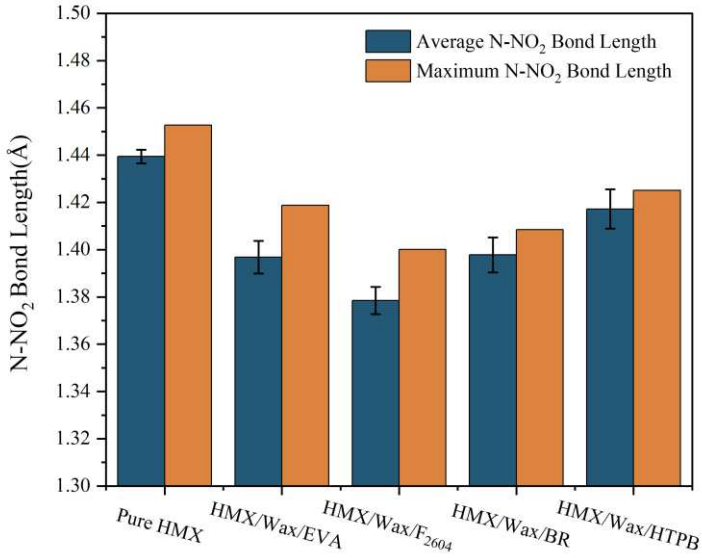


Fig. 8 Trigger bond length distribution of HMX and HMX/Wax/Binder

Comparison shows that for all HMX composite systems added with polymer binder and microcrystalline wax, the average N-NO_2 trigger bond length is shortened by 2.24%-4.23% and the maximum bond length is reduced by 1.90%-3.62%, both values are significantly lower than the benchmark of pure HMX. This result corroborates from the molecular level that the composite coating is not a simple physical barrier, but generates structural constraint through non-bonded interactions between HMX crystal surfaces and binder chains. The flexible polymer can adaptively spread along HMX crystal faces, disperse external mechanical energy, and suppress the non-uniform stretching of N-NO_2 bonds. This confines trigger bonds within a more stable short-bond range, elevates the bond homolytic dissociation activation energy barrier, and ultimately achieves desensitization of the system sensitivity.

In terms of constraint capability, the F_{2604} system presents the minimum values of both average and maximum trigger bond lengths among all tested groups, delivering the best desensitization effect. Even for the HTPB system with the weakest constraint performance, its maximum N-NO_2 bond length is only 1.4251 Å, which is far lower than the threshold of 1.4527 Å for pure HMX. The difference in constraint capability can be attributed to the polarity distinction of binders: the strongly electronegative fluorine atoms on the main chain of F_{2604} form stronger non-bonded interactions with the nitro groups of HMX, leading to a prominent interfacial adsorption-locking effect. In contrast, non-polar HTPB has relatively weak interactions with the polar HMX surface, resulting in a more limited constraint effect on trigger bonds. Notably, the ranking of average bond length is not fully consistent with that of maximum bond length, indicating that the core role of the binder is not only regulating the global bond length distribution, but more importantly, suppressing the locally distributed ultra-long weak bonds. The highly stretched high-risk N-NO_2 bonds, which act as sensitivity hot spot precursors in pure HMX, can have their

upper limit of bond length significantly reduced by the interfacial constraint of the binder.

3.4 Mechanical Property

The mechanical properties are calculated via the Mechanical Properties function in the Forcite module of Materials Studio. The elastic stiffness coefficients and derived mechanical property indices of three composite systems, namely HMX/Wax/binder, AP/Wax/binder and Al-Li alloy/Wax/binder, are summarized in this work. A systematic analysis is conducted based on the Voigt-Reuss-Hill averaging scheme. The physical significance of core evaluation parameters clearly corresponds to the mechanical response characteristics of materials in different dimensions. A higher bulk modulus (K) represents better compression bearing capacity, a larger shear modulus (G) indicates stronger rigidity against shear deformation, and a higher tensile modulus (E) reflects greater resistance to elastic deformation under external loading. Poisson's ratio (γ) is used to characterize the lateral expansion behavior under uniaxial loading. The Cauchy pressure (C_{12}-C_{44}) and the modulus ratio (K/G), serving as two core indicators for ductility and mechanical stability evaluation, respectively reflect the bond-dominated deformation tendency and characterize the relative strength of bulk compression against shear deformation [34-35].

$$|C_{ij}|=\begin{bmatrix} C_{11} & C_{12} & C_{13} & C_{14} & C_{15} & C_{16} \\ C_{21} & C_{22} & C_{23} & C_{24} & C_{25} & C_{26} \\ C_{31} & C_{32} & C_{33} & C_{34} & C_{35} & C_{36} \\ C_{41} & C_{42} & C_{43} & C_{44} & C_{45} & C_{46} \\ C_{51} & C_{52} & C_{53} & C_{54} & C_{55} & C_{56} \\ C_{61} & C_{62} & C_{63} & C_{64} & C_{65} & C_{66} \end{bmatrix} \tag{4}$$

$$G=\frac{G_V+G_R}{2} \tag{5}$$

$$K=\frac{K_V+K_R}{2} \tag{6}$$

$$K_V=\frac{A+2B}{3},\quad K_R=\frac{1}{3a+6b} \tag{7}$$

$$G_V=\frac{A-B+3C}{5},\quad G_R=\frac{5}{4a-4b+3c} \tag{8}$$

$$A=\frac{C_{11}+C_{22}+C_{33}}{3},\quad a=\frac{S_{11}+S_{22}+S_{33}}{3} \tag{9}$$

$$B=\frac{C_{23}+C_{13}+C_{12}}{3},\quad b=\frac{S_{23}+S_{13}+S_{12}}{3} \tag{10}$$

$$C=\frac{C_{44}+C_{55}+C_{66}}{3},\quad c=\frac{S_{44}+S_{55}+S_{66}}{3} \tag{11}$$

$$S_{ij}=C_{ij}^{-1} \tag{12}$$

$$E = \frac{9KG}{3K + G} \tag{13}$$

$$\gamma = \frac{3K - 2G}{2(3K + G)} \tag{14}$$

Table 2 Independent elastic constants of HMX/Wax/Binder.

	HMX/Wax/EVA	HMX/Wax/ F_{2604}	HMX/Wax/BR	HMX/Wax/HTPB
C_{11}	9.3283	8.2115	8.6476	9.3858
C_{22}	8.5044	8.1029	9.6649	6.9132
C_{33}	8.6294	8.8557	7.6749	4.6398
C_{44}	2.0569	2.4284	2.0645	0.5477
C_{55}	2.1380	2.1000	1.9777	1.0319
C_{66}	2.1613	2.1262	1.7884	0.6262
C_{12}	5.0912	4.4519	5.3309	4.4470
C_{13}	5.2673	4.7723	4.2462	6.5368
C_{23}	4.4918	5.0211	4.4100	4.2439
K	4.1039	3.9087	3.9946	4.8534
G	2.0286	2.0308	1.9378	1.1208
E	5.2248	5.1931	5.0041	3.122
γ	0.2878	0.2786	0.2912	0.3928
C_{12}-C_{44}	3.0343	2.0235	3.2664	3.8993
K/G	2.0230	1.9247	2.0615	4.3304

Note: K is bulk modulus, G is Shear modulus, E is tensile modulus, γ is Poisson's ratio, C_{12}-C_{44} is Cauchy, and K/G is modulus ratio.

By comparing the mechanical properties of four sets of HMX/Wax/Binder systems in Table2, it is found that for the HMX/Wax/EVA system, the K and E are both at the medium-upper level, but the low-order shear elastic coefficients are not synchronously improved. In HMX/Wax/ F_{2604}, all elastic parameters in the main diagonal (C value) are within a reasonable range of continuous transition, no obvious short slab in the overall mechanical parameter distribution. In HMX/Wax/BR, one axial principal elastic coefficient is far higher than the other two orthogonal C-values, forming mismatched principal axial stiffness. In HMX/Wax/HTPB, all the shear elastic coefficients are at the lowest positions among the four groups. E that directly reflects the overall load-bearing capacity is significantly low.

Compared with the other three systems, HMX/Wax/ F_{2604} exhibits more remarkable comprehensive advantages in the collaborative adaptability of mechanical properties. Its G and E synchronously reach the highest-level range among the four groups. On the premise of not losing the overall structural strength, the value of γ is effectively reduced. Meanwhile, the two core plasticity criteria, Cauchy pressure and K/G ratio, are both in the optimal interval of the four groups. The overall mechanical response is closer to the ideal isotropic characteristic, and the potential risk of shear localization failure and brittle fracture is relatively lower, which can provide more stable mechanical support for the energetic composite system to adapt to complex working conditions.

Table 3 Independent elastic constants of AP/Wax/Binder.

	AP/Wax/EVA	AP/Wax/ F_{2604}	AP/Wax/BR	AP/Wax/HTPB
C_{11}	6.9565	12.0841	11.0894	8.2115
C_{22}	10.7367	19.1973	18.1299	8.1029
C_{33}	10.6325	9.6498	8.8949	8.8557
C_{44}	4.4496	4.5039	4.5196	2.4284
C_{55}	4.2251	4.9670	5.3537	2.1000
C_{66}	3.5316	4.9729	4.5662	2.1262
C_{12}	2.6955	4.6501	4.3712	4.4519
C_{13}	2.5804	4.4623	3.7127	4.7723
C_{23}	2.9306	3.8118	3.1417	5.0211
K	3.5047	5.3171	5.0115	3.8899
G	3.2575	4.2273	4.3257	0.5547
E	7.4609	10.0251	10.0776	1.5886
γ	0.1452	0.1858	0.1649	0.4319
C_{12}-C_{44}	-1.7541	0.1462	-0.1484	8.1879
K/G	1.0759	1.2578	1.1585	7.0126

Note: K is bulk modulus, G is Shear modulus, E is tensile modulus, γ is Poisson's ratio, C_{12}-C_{44} is Cauchy, and K/G is modulus ratio.

By comparing the mechanical parameters of the four AP/Wax/binder systems in Table3, the AP/Wax/EVA system has well-coordinated C_{11}, C_{22}, C_{33} values with upper-medium K and E, yet its C_{44}, C_{55}, C_{66} are not synchronously enhanced, leading to potential shear stress concentration under multi-axis loads. The AP/Wax/BR system shows prominent uniaxial tensile stiffness with one principal C-value much higher than the others, but poor axial stiffness coordination. The AP/Wax/HTPB system has the lowest shear elastic coefficients in all four

groups, and its overall load-bearing capacity reflected by E is remarkably low. As the optimal selection, the AP/Wax/ F_{2604} system overcomes the shear stiffness limitation of EVA, eliminates the uniaxial overloading anisotropy problem of BR, and solves the global low shear parameter defect of HTPB. Its minimum 3D principal stiffness deviation optimizes the interface stress transfer path, makes G and E reach the top level synchronously. Cauchy pressure and K/G ratio both fall in the optimal interval, with nearly isotropic mechanical response and the lowest risk of shear localization and brittle fracture, which provides the most stable mechanical support for the energetic composite under complex working conditions.

Table 4 Independent elastic constants of Al-Li alloys/Binder/Wax.

	Al-1Li/ F_{2604}/Wax	Al-2Li/ F_{2604}/Wax	Al-3Li/ F_{2604}/Wax	Al-4Li/ F_{2604}/Wax	Al-5Li/ F_{2604}/Wax
C_{11}	64.688	64.3042	39.2963	39.3389	53.5627
C_{22}	41.4671	40.8033	29.4118	29.2364	37.0402
C_{33}	1.6576	3.3788	2.0177	0.0806	0.6023
C_{44}	10.0154	6.5065	5.1659	4.4826	8.1206
C_{55}	4.7312	6.3559	2.1767	2.4522	3.5067
C_{66}	15.2916	15.7913	10.1418	9.9852	13.0979
C_{12}	21.0583	21.192	13.2543	13.4969	17.4999
C_{13}	5.3652	3.3128	2.2958	2.3374	4.1111
C_{23}	9.8978	5.8448	4.2792	4.6982	7.2134
K	7.9510	7.6084	5.3461	5.1631	6.5864
G	0.1735	0.1255	0.2091	0.1066	0.1003
E	0.5168	0.3746	0.6193	0.3176	0.2995
γ	0.4892	0.4918	0.4807	0.4897	0.4924
C_{12}-C_{44}	42.0014	41.9520	29.5416	29.2295	37.0018
K/G	45.8233	60.6030	25.5635	48.4326	65.6438

Note: K is bulk modulus, G is Shear modulus, E is tensile modulus, γ is Poisson's ratio, C_{12}-C_{44} is Cauchy, and K/G is modulus ratio.

A comparison of mechanical parameters for five Al-Li alloy/ F_{2604}/Wax systems in Table 4 shows that, Al-1Li exhibits uneven Z-direction axial stiffness and an elevated K/G ratio, Al-2Li presents a slightly reduced shear modulus and higher K/G ratio, Al-4Li delivers near-zero Z-direction axial modulus, lowered shear properties and further increased K/G ratio, while Al-5Li shows coordinated principal stiffness and fluid-like low-stiffness response. Among all groups, Al-3Li/ F_{2604}/Wax fully satisfies the elasticity positive-definite criterion, with its anisotropy

deviation, multiphase interface stress transfer efficiency and bulk-shear modulus matching all fitting the engineering requirements of energetic coating materials. This system balances sufficient compression resistance and shear deformation resistance, with both Cauchy pressure and K/G ratio located in the reasonable range for structural stability and plastic deformability, presenting relatively low risk of shear localization and brittle fracture and better adaptability to extreme complex service conditions.

3.5 Detonation performance

Detonation performance calculations for HMX(AP)-based PBXs were performed using the EXPLO-5 code. The standard molar enthalpy of formation ($\Delta_f H_m^\theta$) reflects the thermodynamic stability of the formulation and influences the magnitude of detonation heat. Density (ρ) directly determines the energy density per unit volume of the charge and the energy-carrying capacity of the detonation wave. Oxygen balance (OB_{CO2}) reflects the matching between oxidizers and combustible components in the formulation, influencing the proportion of stable species such as CO_2, H_2O, and N_2 in the detonation products as well as the completeness of energy release. Detonation velocity (v_D) and detonation pressure (P_D) characterize the propagation speed of the detonation wave and the pressure at the end of the reaction zone, respectively, and serve as key indicators of detonation intensity and work capacity. Detonation heat (Q_D) and detonation temperature (T_D) describe the total heat released by the detonation reaction and the thermodynamic temperature, while the total volume of detonation gases (V_D) and the average molecular weight of detonation gas products (M_D) reflect the amount of high-temperature gas generated and its expansion work capacity. Together, these parameters provide a comprehensive evaluation of the energy output characteristics of composite energetic systems [36-39].

In the HMX-based PBXs, the differences in detonation performance among the four binder formulations. The HMX/Wax/BR and HMX/Wax/HTPB systems both have a density of 1.83 $g \cdot cm^{-3}$, oxygen balances of -34.04% and -33.75%, and detonation velocities below 8900 $m \cdot s^{-1}$, with detonation pressures within a narrow range of 33.2-33.4 GPa, indicating similar overall performance. The HMX/Wax/EVA system shows a slight increase in density to 1.84 $g \cdot cm^{-3}$, a detonation velocity of 8871.52 $m \cdot s^{-1}$, and a detonation pressure of 33.41 GPa, representing a modest improvement over the former two, but it remains constrained by the oxygen deficiency. In contrast, the HMX/Wax/F_{2604} system exhibits obvious overall advantages, with a density of 1.89 $g \cdot cm^{-3}$ and an improved oxygen balance of -26.35%, corresponding to a markedly reduced oxygen deficiency. The optimized oxygen balance enables carbon and hydrogen to be converted more completely into CO_2 and H_2O during the detonation reaction, releasing more chemical energy. Notably, although the standard molar enthalpy of formation of the F_{2604} formulation is -

13.03kJ·mol^{-1}, the improved oxygen balance plays the dominant role in enhancing the energy release. Meanwhile, the high density achieved by the incorporation of fluorine atoms enhances detonation wave propagation and energy-carrying capacity, increasing the detonation velocity to 9110.99 m·s^{-1}, about 2.7% higher than that of the EVA system, and the detonation pressure to 36.22 GPa, about 8.6% higher than those of the BR and HTPB systems. These results indicate that F_{2604} achieves synergistic enhancement of energy release efficiency and detonation intensity in HMX-based systems by reducing the proportion of combustible hydrocarbon elements, optimizing the oxygen balance, and increasing the charge density, making it the formulation with the best overall performance.

In the AP-based composite energetic systems, the AP/Wax/BR and AP/Wax/HTPB systems benefit from hydrocarbon binders that provide reducing components well matched to the oxidizing capacity of AP, resulting in oxygen balances closer to the ideal state and highly complete detonation reactions. In the AP/Wax/EVA system, the oxygen atoms in the binder molecule diminish its reducing capacity, lowering the detonation velocity and the detonation pressure, slightly below those of the former two. AP/Wax/ F_{2604} system achieves a density of 1.94 g·cm^{-3}, the highest among all formulations, and its oxygen balance increases to 27.07%, indicating a distinctly positive oxygen balance. In addition, further suppressing the detonation heat output due to the higher thermodynamic stability of the reactants. However, fluorine in the F_{2604} system reduces the formation of high-molecular-weight hydrocarbon fragments, lowering the average molecular weight of detonation gas products to a minimum and improving the expansion work efficiency of the high-temperature gases. The high density also ensures that the charge still delivers a considerable total energy output per unit volume. Overall, in AP-based systems, F_{2604} significantly improves the mechanical stability and long-term service performance of the charge at the cost of a small and controllable reduction in detonation energy, owing to its high density, low product molecular weight, and low-signature characteristics, making it a promising preferred formulation for engineering applications.

Table 5 Detonation parameters of HMX/Wax/Binder and AP/Wax/Binder.

Model	ρ/g·cm^{-3}	$\Delta_f H_m^\theta$ /kJ/mol	OB_{CO2}/ %	v_D/m·s^{-1}	Q_D/kJ·kg^{-1}	T_D/K	P_D/GPa	V_D/dm^3·kg^{-1}	M_D/g·mol^{-1}
HMX/Wax/EVA	1.84	46.52	-32.36%	8871.52	-5405.59	3453.31	33.41	779.17	28.92
HMX/Wax/ F_{2604}	1.89	-13.03	-26.35%	9110.99	-5506.46	3526.72	36.22	771.45	29.92
HMX/Wax/BR	1.83	76.18	-34.04%	8871.60	-5516.61	3500.97	33.34	780.94	28.67
HMX/Wax/HTPB	1.83	69.60	-33.75%	8853.79	-5467.11	3483.84	33.21	779.45	28.75
AP/Wax/EVA	1.88	-309.24	21.07%	7480.79	-2792.96	2482.27	22.78	878.52	27.84

AP/Wax/ F_{2604}	1.94	-368.78	27.07%	7273.26	-2127.98	2104.63	21.14	877.15	27.88
AP /Wax/BR	1.87	-279.57	19.39%	7598.68	-3114.94	2662.07	23.69	878.59	27.83
AP/Wax/HTPB	1.87	-286.15	19.68%	7558.58	-3029.76	2618.01	23.40	877.08	27.88

Note: ρ is the density of the explosives; OB_{CO2} is the oxygen balance; v_D is the detonation velocity; Q_D is the heat of detonation; T_D is the explosion temperature; P_D is the detonation pressure; V_D is the total generation of detonation gases; M_D is the average molecular weight of detonation gas products.

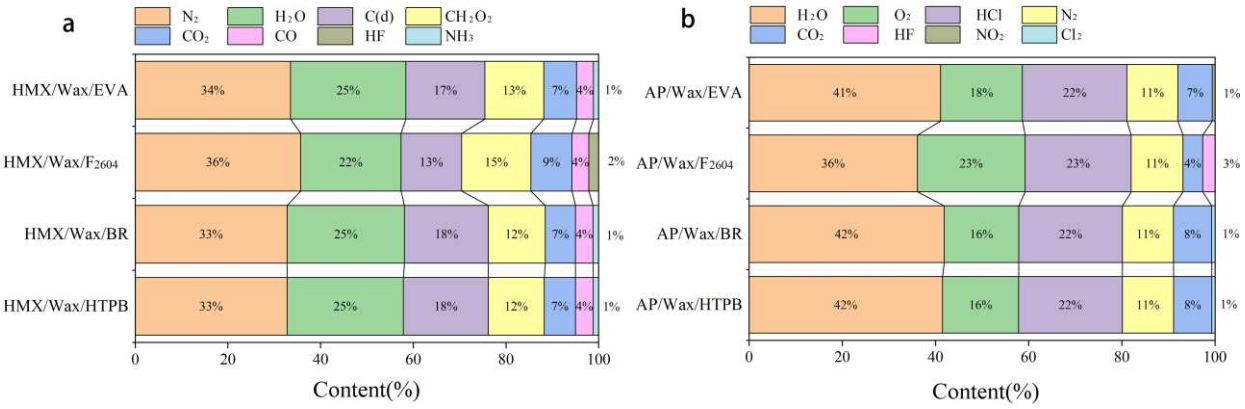


Fig. 9 Detonation products of HMX/Wax/Binder and AP/Wax/Binder.

The detonation products of AP-based composite systems are dominated by H_2O, HCl and O_2, and the chemical structure differences of different binders exert a significant influence on product distribution, show in the Fig.9. The H_2O proportion in AP/Wax/EVA, AP/Wax/BR, AP/Wax/HTPB systems maintain a high range from 40.69% to 41.39%, while the H_2O proportion in AP/Wax/ F_{2604} system decreases to 35.75%, which indicates that rubber-based binders with high hydrogen content show better oxygen balance matching performance with ammonium perchlorate, and can convert hydrogen elements into water molecules more fully. The O_2 proportion in AP/Wax/ F_{2604} system reaches 22.88%, which is much higher than the range of 15.81% to 17.40% in the other three systems. This phenomenon is related to the fluorine-containing characteristic of F_{2604} binder, which changes the decomposition pathway of ammonium perchlorate and causes part of the oxidant to generate residual oxygen directly without full participation in the reaction.

The distribution characteristics of detonation products in HMX-based composite systems are markedly different from those of AP-based systems. Since the system does not contain chlorine-containing components such as AP, no chlorine-related substances are observed in products, and the core components are N_2, H_2O and elemental solid carbon, while the proportions of nitrogen-containing and carbon-containing products including CO, CO_2 and NH_3 are also significantly higher than those in AP-based systems. Under the effect of different binders, the N_2

proportion in HMX/Wax/ F_{2604} system reaches 35.69%, which is notably higher than the range from 32.8% to 33.5% in the other three systems, suggesting that F_{2604} has better chemical compatibility with HMX and the conversion efficiency of nitrogen elements to nitrogen gas during detonation is higher.

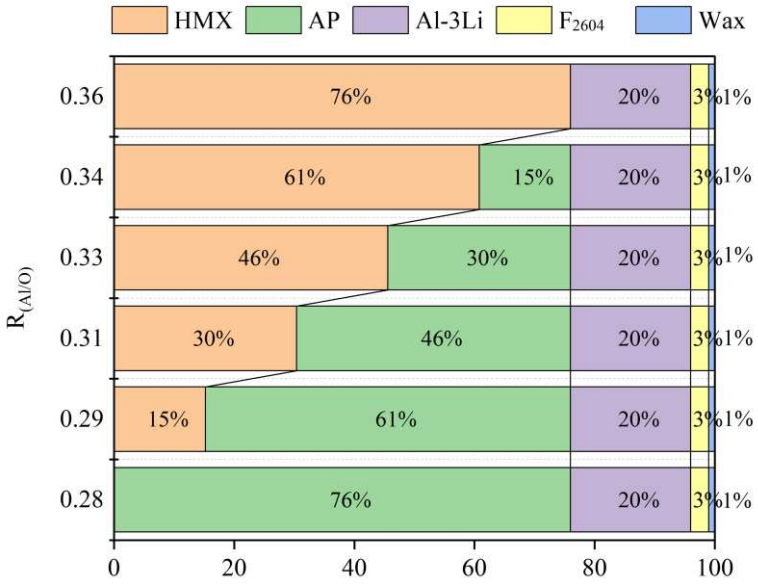


Fig. 10 Formulation of HMX/AP/Al-3Li composite explosives

The formulation selection criteria prioritize optimal compatibility between each component, binder, wax and other constituents, alongside maximum bonding energy, cohesive energy density, intermolecular interaction strength and minimum bond length, while maintaining balanced mechanical properties and satisfactory detonation performance. An optimized Al-3Li composite explosive formulation was thus determined, with wax accounting for 1 wt% of the total HMX and AP mass, and F_{2604} accounting for 3 wt% of the total formulation mass.

Further research demonstrates that optimal detonation performance (e.g. significantly enhanced shock wave energy) is typically obtained at an aluminium-to-oxygen ratio ($R_{Al:O}$) ranging from 0.25 to 0.4[40], where $R_{Al:O}$ is defined as the molar ratio of Al atoms per unit mass of the composite explosive to total O atoms supplied by the explosive and oxidizer. By adjusting the mass ratio of HMX to AP, a series of formulations with progressively increasing $R_{Al:O}$ were designed, as illustrated in Figure 10.

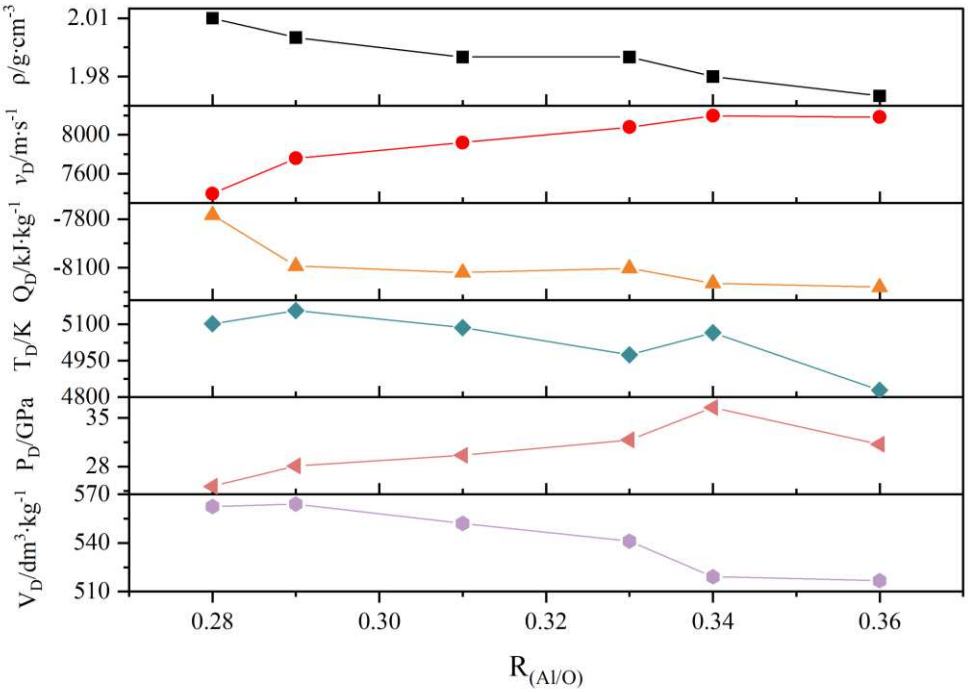


Fig. 11 Performance parameters of HMX/AP/Al-3Li composite explosives

The energy performance parameters in Figure 11 show that theoretical density decreases with rising Al/O ratio, reflecting system density dilution. Q_D peaks at $R_{Al:O}$ is 0.28 then declines, while v_D follows an opposite upward trend. Formulations with higher HMX content deliver the maximum total detonation heat via its ultrahigh energy density, and the subsequent rise in AP proportion supplies abundant reactive oxygen species to further boost reaction efficiency. Combined with Table 5, this series of Al-Li composite explosives shows significantly higher detonation heat than pure AP-based and HMX-based PBX, attributed to the after burning effect of proper metal fuel that enhances total energy release.

T_D fluctuates and reaches its maximum at $R_{Al:O}$ is 0.29, where Al-Li particles match detonation-generated active oxygen optimally, avoiding sensible heat dilution by excess oxygen or heat loss from incomplete fuel-oxygen reaction. P_D follows a rise-fall trend, incomplete oxidation occurs at low $R_{Al:O}$, while the drop above 0.34 arises from insufficient oxidizer oxygen to fully react all metal particles at the detonation front. Unreacted particles occupy extra product space and reduce peak pressure. V_D yield decreases with rising $R_{Al:O}$. With fixed total metal fuel content, higher AP proportion replaces more gas-productive HMX, lowering the fraction of small gaseous products N_2, CO, H_2O and reducing total gas output per unit mass explosive.

4 Conclusions

This work systematically investigates the tuning effect of a dual-layer wax-binder architecture and gradient lithium doping on the safety and energy performance of AP-containing HMX-based aluminized PBXs, using

molecular dynamics simulations and EXPLO-5 detonation property calculations. An HMX-based polymer-bonded explosive (PBX) using F_{2604} as the binder and incorporating 3 wt% lithium is capable of forming defect-free, high-adhesion coating structures, providing a solid theoretical basis for the design of high-energy, low-sensitivity PBX containing Al-Li alloys.

(1) F2604 was selected as the optimal adhesive with the highest wax compatibility, providing a maximum binding energy of 13261 kJ·mol^{-1} and a cohesive energy density of 6.03×10^{8} kJ·cm^{-3} in the HMX/Wax/F_{2604} system. RDF results confirmed that interfacial adhesion was dense and uniform in all three sandwich-structure configurations; the HMX/wax/F_{2604} interface was dominated primarily by weak hydrogen bonds and van der Waals forces, whilst the AP/wax/F_{2604} interface comprised medium-strength hydrogen bonds, as well as weak hydrogen bonds and van der Waals forces. In this dual-layer coating system, the N-NO_2 trigger bond length of HMX remains consistently well below the critical decomposition threshold, thereby effectively suppressing deformation of the sensitive bonds under external excitation. The formulation combined with F2604 and microcrystalline wax achieved the optimal trigger bond shortening effect, with the average N-NO_2 bond length shortened by 4.23% and the maximum bond length reduced by 3.62%. In both the HMX-based and AP-based systems, F2604 exhibited a near-isotropic mechanical response, with the lowest potential risk of shear localization and brittle fracture.

(2) The interface between the Al-Li alloy, wax and F_{2604} is primarily governed by weak hydrogen bonds and van der Waals forces, and this system exhibits the highest interfacial interaction strength among all test groups. The moderately lithium-doped system (3 wt%) achieved a peak binding energy of 5250 kJ·mol^{-1} and a cohesive energy density of 5.68×10^{9} kJ·m^{-3}. The Al-3Li/F_{2604}/wax composite fully satisfies the criteria for elastic positive definiteness; its anisotropy deviation, multiphase interface stress transfer efficiency and the ratio of bulk modulus to shear modulus are all well-matched, endowing this system with excellent mechanical buffering and hot-spot suppression properties.

(3) The HMX/AP/Al-3Li composite explosive, as $R_{Al/O}$ rises, more AP-supplied reactive oxygen improves metal fuel reaction efficiency, forming a trend of decreasing Q_D, increasing v_D, and both T_D and P_D peak at $R_{Al/O}$ is 0.34 with V_D at its minimum.

Conflicts of interest

There are no conflicts of interest to declare

References

[1] D. Drouet, D. Picart, P. Bailly, E. Bruneton, Plastic dissipation and hot-spot formation in HMX-based PBXs subjected to low velocity impact, Propellants, Explos., Pyrotech. 45 (2020) 1884-1893,

https://doi.org/10.1002/prep.202000060.

[2] H. Duan, Y. Wu, K. Yang, F. Huang, Numerical simulation of drop weight impact sensitivity evaluation criteria for pressed PBXs, Def. Technol. 19 (2023) 76-90, https://doi.org/10.1016/j.dt.2022.01.013.

[3] Y. Li, W. Xu, F. Guo, et al., Preparation and characterization of PANI surface modified HMX/F2602 microcapsule composites, Propellants, Explosives, Propellants Explos. Pyrotech. 47 (10) (2022) e202200084, https://doi.org/10.1002/prep.202200084.

[4] W. Wu, W. Liu, X. Fu, et al., Construction of HMX/FOX-7 composite microspheres with controlled microstructures using continuous self-assembly spray drying: To improve safety and combustion performance, Materials Chemistry and Physics. 339 (2025) 130795-130810, https://doi.org/10.1016/j.matchemphys.2024.130795.

[5] B. Peng, W. Bian, G. He, et al., Directional design of interface and thermal performance for CL-20 using hollow fiber embed in desensitizer membranes, Chemical Physics Letters. 858 (2025) 141747-141758, https://doi.org/10.1016/j.cplett.2024.141747.

[6] H. JING, Y. WU, Q. ZHAO, et al. Study on Preparation, Characterization and Acousto-Optic Properties of Stearic Acid Coated Aluminum Powder[J]. CBRN Defense, 2023, 2(6): 72-76. https://doi.org/10.20179/j.cnki.fhyj.2023.06.009

[7] C. Hou, M. Liu, C. Xu, et al., Preparation and characterization of CL-20/NTO/Estane5703 composite microspheres by spray drying, AIP Advances. 12 (3) (2022) 035049-035056, https://doi.org/10.1063/5.0083271.

[8] W. Xu, J. Wang, X. Chang, et al., Study on the modification of HMX/TPU composites with metal-phenolic network, Polymer Engineering and Science. 64 (5) (2024) 2268-2277, https://doi.org/10.1002/pen.26762.

[9] Y. Yang, X. Li, Y. Sun, et al., Preparation and characterization of HMX/EVA/hBNNSs micro-composites with improved thermal stability and reduced sensitivity, Defence Technology. 17 (2) (2021) 650–656, https://doi.org/10.1016/j.dt.2020.06.013.

[10] X. Zhou, L. Huang, X. Liu, et al., Combustion characteristics of Al-Li alloy powder and its application in solid propellant, Journal of Physics: Conference Series. 2478 (3) (2023) 032067, https://doi.org/10.1088/1742-6596/2478/3/032067.

[11] W. Xiong, Y. Liu, T. Zhang, et al., Effect of Al-Li alloy on the combustion performance of AP/RDX/Al/HTPB propellant, Aerospace. 10 (3) (2023) 222, https://doi.org/10.3390/aerospace10030222.

[12] W. Han, X. Hu, Corrosion of Al-Li alloy melt on oxide refractories, Anti-Corrosion Methods and Materials. 70

(5) (2023) 229-235, https://doi.org/10.1108/ACMM-03-2023-2287.

[13] B.C. Terry, I.E. Gunduz, M.A. Pfeil, et al., A mechanism for shattering microexplosions and dispersive boiling phenomena in aluminum-lithium alloy based solid propellant, Proceedings of the Combustion Institute. 36 (2) (2017) 2309-2316, https://doi.org/10.1016/j.proci.2016.06.183.

[14] C. Li, W. Wang, X. Zeng, C. Liu, R. Sun, Emerging low-density polyethylene/paraffin wax/aluminum composite as a form-stable phase change thermal interface material, Int. J. Miner. Metall. Mater. 30 (2023) 772-781, https://doi.org/10.1007/s12613-022-2565-6.

[15] S. Tang, M. Zou, Preparation of al-5Li@FSG powders through fluorination-energetic modification to improve the comprehensive performance of alloy powders, Chem. Eng. J. 506 (2025) 160210, https://doi.org/10.1016/j.cej.2025.160210.

[16] Z. Sun, L. Yang, H. Li, M. Mei, L. Ye, J. Fan, W. Zhu, Thermal decomposition of core–shell-structured RDX@AlH_3, HMX@AlH_3, and CL-20@AlH_3 nanoparticles: Reactive molecular dynamics simulations, Nanomaterials. 14 (22) (2024) 1859, https://doi.org/10.3390/nano14221859.

[17] F. Gao, J. Jing, W. Cheng, H. Song, S. Li, Z. Zhang, J. Wang, C. An, Molecular dynamics simulation of bilayer core-shell structure of CL-20 surface-modified by polydopamine coated with polymer binder, Materials Today Communications. 37 (2024), https://doi.org/10.1016/j.mtcomm.2023.107099.

[18] M. Chen, J. Li, B. Wang, X. Lu, B. Duan, N. Liu, Molecular dynamics simulation on ε-CL-20 based PBXs with chain-extended poly(3,3-bis(azidomethyl)oxetane), Comput. Theor. Chem. 1214 (2022) 113762, https://doi.org/10.1016/j.comptc.2022.113762.

[19] G. He, et al., Polymer bonded explosives (PBXs) with reduced thermal stress and sensitivity by thermal conductivity enhancement with graphene nanoplatelets, Compos. Sci. Technol. 131 (2016) 22-31, https://doi.org/10.1016/j. compscitech.2016.05.009.

[20] B.-h. Duan, X.-m. Lu, H.-c. Mo, et al., Fabrication of CL-20/HMX cocrystal@melamine–formaldehyde resin core–shell composites featuring enhanced thermal and safety performance via in situ polymerization, International Journal of Molecular Sciences. 23 (12) (2022) 6710–6726, https://doi.org/10.3390/ijms23126710.

[21] B. Duan, H. Mo, B. Tan, et al., Interfacial reinforcement of core-shell HMX@energetic polymer composites featuring enhanced thermal and safety performance, Defence Technology. 31 (2024) 387-399, https://doi.org/10.1016/j.dt.2023.11.005.

[22] Q. Lan, H. Zhang, Y. Ni, J. Chen, H. Wang, Thermal decomposition mechanisms of LLM-105/HTPB plastic-bonded explosive: ReaxFF-lg molecular dynamics simulations, J. Energ. Mater. 41 (2023) 269-290,

https://doi.org/10.1080/07370652.2021.1968071.

[23] Z. Zhang, Z. Lin, Y. Guo, et al., Preparation of μ-HMX/C-based composite energy composite microspheres by microdroplet technology, Langmuir. 40 (26) (2024) 13676-13687, https://doi.org/10.1021/acs.langmuir.4c01087.

[24] H. He, G. Li, X. Zhu, H. Duan, J. Yu, R. Liu, Y. Qu, Y. Yin, Suppressed friction-induced temperature rise at energetic β-HMX crystal interfaces by wax coating, Friction. 13 (2025) 9441063, https://doi.org/10.26599/FRICT.2025.9441063.

[25] J. Zhou, B. Wu, R. Zhu, Y. Guo, J. Shi, C. An, J. Wang, High-quality and homogeneous HMX-based aluminized explosives using droplet microfluidic technology, Energetic Mater. Front. 3 (2022) 219–225, https://doi.org/10.1016/j.enmf.2022.01.004.

[26] H. Lin, S.G. Zhu, L. Zhang, X.H. Peng, P.Y. Chen, H.Z. Li, Intermolecular Interactions, Thermodynamic Properties, Crystal Structure, and Detonation Performance of HMX/NTO Co-crystal Explosive, Int. J. Quantum Chem. 113 (10) (2013) 1591–1599, https://doi.org/10.1002/qua.24369.

[27] P.J. Flory, Principles of Polymer Chemistry, Cornell University Press, Ithaca, 1953.

[28] J. Karwounopoulos, M. Wieder, S. Boresch, Relative binding free energy calculations with transformato: A molecular dynamics engine-independent tool, Front. Mol. Biosci. 9 (2022) 954638, https://doi.org/10.3389/fmolb.2022.954638.

[29] F. Chen, Y.Y. Ren, L. He, C.W. An, S.F. Wen, F.F. Shen, Molecular dynamics simulation of the interface interaction and mechanical properties of PYX and polymer binder, AIP Adv. 12 (2022) 025307, https://doi.org/10.1063/5.0080679.

[30] Z.H. Yu, X.L. Song, Y. Wang, Z.P. Cheng, C.W. An, Theoretical investigations on CL-20/TNBA co-crystal explosive via density functional method and molecular dynamics method, Mater. Today Commun. 37 (2023) 107388, https://doi.org/10.1016/j.mtcomm.2023.107388.

[31] Y. Zhang, Z. Yu, H. Xu, L. Zhou, X. Zhang, W. Peng, P. Zhang, H. Chen, Z. Zhuang, Molecular dynamics simulation of NTO/TNPyO co-crystals for targeted acidity regulation of NTO, Langmuir. 42 (26) (2026) 18865-18879, https://doi.org/10.1021/acs.langmuir.6c01475.

[32] H. Zhao, W. Wu, S. Xu, H. Wang, T. Wang, X. Huang, N. Wang, H. Hao, Structure-performance relationship of CL-20-HMX-based composite energetic materials revealed by molecular simulation, Results Eng. 29 (2026) 109926, https://doi.org/10.1016/j.rineng.2026.109926.

[33] Y. Zhang, R. Liu, W. Cao, Q. Pei, F. Zhao, X. Zhang, T. Zhang, C. Wu, X. Liu, S. Xu, Effects of RDX and

HMX on the thermal stability properties of modified double-base propellants, FirePhysChem. 5 (2025) 420–427, https://doi.org/10.1016/j.fpc.2025.01.006.

[34] B. Liu, X.J. Wang, X.Y. Bu, First principles investigations of structural, electronic and elastic properties of ammonium perchlorate under high pressures, Acta Phys. Sin. 65 (2016) 126102, https://doi.org/10.7498/aps.65.126102.

[35] K. Moch, N.P. Bailey, Isomorph invariant dynamic mechanical analysis: A molecular dynamics study, Phys. Rev. Mater. 6 (2022) 085602, https://doi.org/10.1103/PhysRevMaterials.6.085602.

[36] Y. Ikeda-Fukazawa, Structure of absorbed water in cis-1,4-polyisoprene rubber and its effect on properties of polymers, Thermochim. Acta. 729 (2023) 179619, https://doi.org/10.1016/j.tca.2023.179619.

[37] L. Min, B. Zhang, Theoretical insights into the dissociation and oxidation of ethylene during vinyl acetate synthesis, Catal. Today. 429 (2024) 114177, https://doi.org/10.1016/j.cattod.2023.06.023.

[38] N.V. Muravyev, K.A. Monogarov, D. Prokopyev, A.A. Bragin, L. Galfetti, L.T. DeLuca, A.N. Pivkina, Macro- vs microcrystalline wax: interplay of evaporation and decomposition under pressure variation, Energy Fuels. 31 (8) (2017) 8534-8539, https://doi.org/10.1021/acs.energyfuels.7b00895.

[39] F. Cataldo, Thermochemistry of sulfur-based vulcanization and of devulcanized and recycled natural rubber compounds, Int. J. Mol. Sci. 24 (3) (2023) 2623, https://doi.org/10.3390/ijms24032623.

[40] ZHOU Lin, YANG. Qi-xian. The Effect of Al/O Ratio on Underwater Explosion Shock Wave of Aluminium-containing Explosives, Acta Armamentarii. 27(2) (2006)235-238. (in Chinese), https://doi.org/10.12382/bgxb.2008.0916.